Charge State Dependent Energy Deposition by Ion Impact

R. E. Lake,[1,2,*] J. M. Pomeroy,[1] H. Grube,[1] and C. E. Sosolik[2]

[1]*Physical Measurement Laboratory, National Institute of Standards and Technology, Gaithersburg, Maryland, 20899 USA*
[2]*Department of Physics and Astronomy, Clemson University, Clemson, South Carolina, 29634 USA*

(Received 19 April 2011; published 5 August 2011)

We report on a measurement of craters in thin dielectric films formed by Xe^{Q+} $(26 \leq Q \leq 44)$ projectiles. Tunnel junction devices with ion-irradiated barriers were used to amplify the effect of charge-dependent cratering through the exponential dependence of tunneling conductance on barrier thickness. Electrical conductance of a crater $\sigma_c(Q)$ increased by 4 orders of magnitude (7.9×10^{-4} μS to 6.1 μS) as Q increased, corresponding to crater depths ranging from 2 to 11 Å. By employing a heated spike model, we determine that the energy required to produce the craters spans from 8 to 25 keV over the investigated charge states. Considering energy from preequilibrium nuclear and electronic stopping as well as neutralization, we find that at least (27 ± 2)% of available projectile neutralization energy is deposited into the thin film during impact.

DOI: 10.1103/PhysRevLett.107.063202 PACS numbers: 34.35.+a, 79.20.Rf, 85.30.Mn

Craters formed by energetic projectile impacts record both the energy deposited in a medium and the mechanisms by which that energy is transferred. On the macroscopic scale, planetary scientists use meteor impact sites to reconstruct the mass and velocity of the impinging meteorite [1]. Similarly, on the atomic scale, the surface modifications formed by ion-surface impacts form a record of both the elastic and inelastic pathways for energy loss and possess distinct shapes that vary as a function of ion velocity, ion charge state, and the target material properties [2–5]. Sputter damage from singly charged ions, for example, is governed by kinetic energy loss to target nuclei and electrons along the ion's path [6] (and references therein). Accurately predicting this loss channel, which can be achieved over a wide incident energy range through semiempirical models [7], is a key input for many ion-based processing techniques, such as ion milling, ion track formation or etching, lithography, and implantation [6,8,9].

An increase in the initial charge state of an incident ion can open up new pathways for inelastic energy transfer and lead to the formation of irreversible surface modifications even at low kinetic energies [10]. For highly charged ions (HCIs), the electronic potential energy or *neutralization energy* which is the sum of the binding energies of the electrons removed during ionization, drives the inelastic energy transfer. However, the role of neutralization energy in surface modification is poorly understood when compared to defect formation through kinetic energy loss. The ability to harness this pathway in materials processing [11,12] and mitigate its role in important erosion processes [13] such as in fusion reactors requires charge state dependent measurements of energy deposition into a material. Increasing the projectile charge state also enhances the kinetic energy loss to the target material during electronic equilibration [14,15].

In this Letter, we describe measurements of charge state dependent cratering induced by HCI impacts on thin dielectric films. Our results quantify the charge-dependent energy deposition in a solid that leads to the formation of irreversible defects. The scaling of crater depths with Q is measured and compared with a heated spike model to determine the crater formation energy. We partition this energy into kinetic and neutralization contributions and obtain the fraction of the neutralization energy that is deposited into an Al_2O_3 film. Unlike recent work that uses microscopy to determine individual feature sizes [2–5], we utilize electrical measurements of tunnel junctions with HCI-irradiated barriers. The exponential sensitivity of the tunneling conductance to the dielectric thickness within such a junction amplifies the effect of charge-dependent cratering and allows for the extraction of the crater depth. By focusing on modifications to an ultrathin dielectric surface film, we optimize sensitivity to neutralization energy. In addition, we are able to sample crater depths from an ensemble of input sites simultaneously within a single electrical measurement when the film is embedded in a tunnel junction. Although raised hillocks are frequently observed by scanning probe measurements due to the impact of individual HCIs [10], the increase in tunneling conductance we observe requires a reduction in the thickness of the aluminum oxide barrier. Tunneling current flows preferentially through the thinnest parts of the barrier and the presence or absence of hillocks cannot be measured. HCI irradiation of an exposed tunnel barrier always increases the electrical conductance of a device and this effect can only be explained by decreased barrier thickness from cratering at each impact site.

The neutralization scenario for HCIs at a surface has been discussed in detail previously [16] and is shown schematically in Fig. 1(a). As the ion approaches a critical

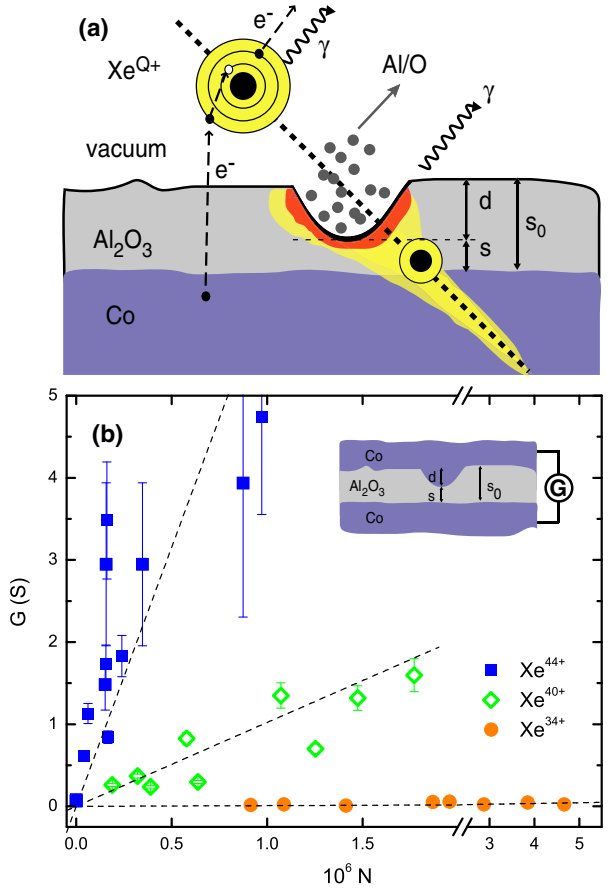

FIG. 1 (color online). (a) Schematic representation of neutralization and heated spike formation scenario for relaxation of a HCI above a metal surface covered with a thin dielectric film [16,37]. The heated spike leading to crater formation occurs during subsurface neutralization. (b) Electrical conductance of a tunnel junction increases linearly with the number of ion impacts. The slope of each line (σ_c) increases with increasing Q. $\sigma_c(Q)$ for $Q = 34, 40, 44$ are (8 ± 3) nS, (3.5 ± 0.6) μS, (6.1 ± 0.3) μS, respectively. Error bars represent experimental uncertainty which, for some data points, is less than the symbol size.

distance of a few nanometers from the surface, electrons from the metal are captured into highly excited states of the projectile forming a neutral "hollow atom" [17]. Only a small fraction ($< 10\%$) [18,19] of the neutralization energy can be dissipated above the surface through Auger electron and x-ray emissions, even for the case of slow HCIs ($v < v_{\mathrm{bohr}}$). Upon entering the solid the evolving HCI is reionized through the "peeling off" of excited electrons [16,20], and the ion remains far from charge state equilibrium. In our experiment, the slowest projectiles have nominal perpendicular velocities $v = 576$ km s^{-1} (neglecting image acceleration) and pass through the 14 Å surface film within 2.5 fs. In comparison, full electronic relaxation requires 7 to 68 fs [21,22]. Therefore, the craters formed in the film are the result of subsurface preequilibrium energy deposition within a short (< 2.5 fs) time window.

The tunnel junction devices were prepared and irradiated at the National Institute of Standards and Technology, electron beam ion trap facility *in situ* with base vacuum pressure $< 3 \times 10^{-8}$ Pa. Each tunnel junction device was grown on a Si oxide substrate with the layer structure (in nm): bottom contact and antiferromagnet pinned layer [2 Co + Ox/21 Co], tunnel barrier [1.1 Al + Ox], magnetic free layer and top contact [10 Co/40 Cu/3 Au]. All layers were deposited by electron beam evaporation where +Ox indicates exposure to oxygen plasma after growth. Shadow masks were used to define the sizes and positions of the thin film electrodes so that each Si oxide chip had 4 devices arranged in crossed wire geometry. After plasma oxidation the Al expands to thickness $s_0 = (14 \pm 1)$ Å [23,24]. HCI irradiation occurred >12 hours after oxidation of the Al layer (following glassy relaxation of the oxide). As a control, one device per chip was left unirradiated. Beams of a single charge Xe^{Q+} were extracted for $26 \leq Q \leq 44$ with kinetic energy $E = 8.1$ keV $\times Q$ onto the Al_2O_3 barriers near normal incidence. Subsequently, the magnetic free layer and top contact were deposited onto the irradiated surface. When devices were completed, the area ($\approx 10^4$ μm^2) of each was measured with optical microscopy. Four-point probe differential resistance measurements were obtained at low bias and corrected for the negative resistance artifacts [25]. The inverse of the corrected resistance measurement is then device conductance G.

In Fig. 1(b) we show the conductance of many devices as a function of ion dose for representative charge states $Q = 34$, 40, 44. Each point is the conductance of one tunnel junction modified by N discrete ion impact sites. G increases linearly as a function of ion dose and each ion creates an individual feature in the barrier during irradiation. $G(N)$ for a particular charge state was fit to the line $G(N) = \sigma_c N + G_0$ where G_0 is the conductance of the device with a pristine barrier as determined from the unirradiated control device and σ_c is the average conductance increase per ion impact. σ_c is positive for all charge states.

The left axis in Fig. 2 displays σ_c values for all charge states. The increase in conductance is due to a reduction of the barrier thickness through charge-dependent cratering. In some cases, the experimental uncertainty expressed by the error bars is smaller than the symbol size. We describe the decreased barrier thickness $s(Q) = s_0 - d$ as a function of ion charge state Q, where s is the barrier thickness at the bottom of a crater after a Xe^{Q+} impact, s_0 is the initial barrier thickness and d is the depth of a crater [Fig. 1(a)]. The craters subsequently become filled with the Co of the top electrode during completion of the device. The tunnel conductance of each crater depends exponentially on the barrier thickness as $\sigma_c(s) \simeq G_0 \exp[-A\sqrt{\phi}s]$, where $G_0 = 2e^2/h \approx 77.5$ μS, h is the Planck constant and $A \approx 1.025$ Å^{-1} eV$^{-(1/2)}$, and e is an elementary charge. G_0 represents the magnitude of conductance for electrons

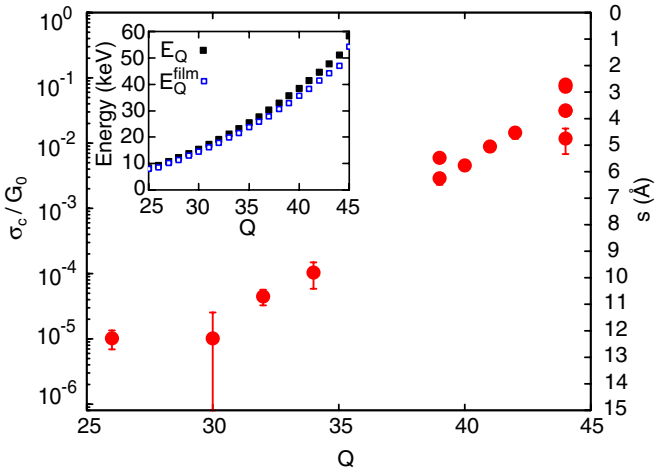

FIG. 2 (color online). $\sigma_c(Q)$ increases by 4 orders of magnitude for charge states between $Q = 26$ and $Q = 44$ where Q is in units of elementary charge. Electrical conductance of each ion impact site increases due to a decrease in barrier thickness after charge-dependent crater formation. Right axis displays the barrier thickness s corresponding to each conductance value from Eq. (1). The inset shows Xe neutralization energy (E_Q) and neutralization energy dissipated within the 14 Å film (E_Q^{film}) assuming exponential charge equilibration.

through a single narrow channel while $\exp[-A\sqrt{\phi}s]$ is the transmission probability. From this expression, s can be written in terms of the measured tunnel conductance,

$$s(\sigma_c) \simeq -\frac{1}{A\sqrt{\phi}} \ln[\sigma_c/G_0]. \quad (1)$$

Conductance does not depend explicitly on the crater radius because tunneling through regions surrounding the bottommost point of the crater is exponentially suppressed. In the limit that s approaches the thickness of a single atom ($d \rightarrow s_0$), conductance through the crater saturates at G_0 and the site behaves as a quantum point contact. Electron tunneling spectroscopy and resistance-temperature measurements confirm that devices remain tunneling after irradiation of the barriers [12]. Extensive dI/dV measurements of irradiated devices indicate that impacts do not cause a significant decrease in barrier height ϕ [26,27]. Furthermore, the four decade span of $\sigma_c(Q)$ with no saturation in conductance demonstrates that charge state dependent cratering decreases the barrier thickness and drives a tunneling conductance increase. All values of σ_c shown in Fig. 2 are below the typical conductance thresholds for the onset of metallic transport through a narrow channel [28].

Using Eq. (1), the barrier thickness that corresponds to each measured σ_c value is extracted. These values are included as a linear scale along the right vertical axis of Fig. 2, with s decreasing from 12 to 3 Å as Q is increased from 26 to 44. This decrease in barrier thickness represents Q-dependent crater formation and we obtain the crater depth d as the difference between s_0 and s at each at each ion impact site. The range of crater depths obtained is 2 to 11 Å. Included as the inset of Fig. 2 is the total neutralization energy E_Q for each charge state (filled symbols), as well as the neutralization energy expected to be lost in the thickness of the film E_Q^{film} (open symbols), assuming an exponential decay of the charge state (discussed below).

The energy required to form a given crater of depth d in the thin film is determined using a heated spike model from Sigmund [29–31]. The ion collision forms a nonequilibrium temperature profile that cools simultaneously through heat conduction to the solid and evaporative heat loss. In particular, it is the temperature dependent evaporation of near-surface atoms from the semi-infinite cylindrical spike around a projectile's trajectory which gives rise to crater formation. After cooling, the final depth of a given crater can be expressed as

$$d(E_{\text{dep}}) = \frac{\beta E_{\text{dep}}(kT_0)^{1/2}}{Us_0} \exp[-U/(kT_0)], \quad (2)$$

where k is the Boltzmann constant, E_{dep} is the total energy deposited in the length s_0, $\beta = k(4\sqrt{2}\pi^{3/2}M^{1/2}\Lambda)^{-1}$ (Λ is the thermal conductivity of the target and M is the mass of a target atom), T_0 is the initial temperature of the spike and U is the surface binding energy per evaporated atom. The heated spike has initial thermal energy $kT_0 = (2/3)E_{\text{dep}}$ [30]. In applying this model to high Q projectiles, both subsurface neutralization energy deposition and preequilibrium nuclear and electronic stopping contribute to spike formation.

Within the heated spike model, we consider heat dissipation through conduction to occur primarily through the Co layer, given its high thermal conductivity compared to the Al_2O_3 thin film. Therefore the thermal conductivity was taken to be the nominal value for Co of $\Lambda = 100\ \text{W K}^{-1}\ \text{m}^{-1}$ [32]. The target mass M was a weighted average between the masses of the Al and O species in stoichiometric Al_2O_3, and the surface binding energy was set at the experimentally determined aluminum displacement threshold of 20 eV [33]. Equations (1) and (2) are connected by the unperturbed barrier thickness s_0 as, $s(\sigma_c) + d(E_{\text{dep}}) = s_0$. For each charge state, E_{dep} was obtained using the measured σ_c value as shown in Fig. 3. For the spike parameters described above, we find that E_{dep} increases from approximately 8 to 25 keV as the projectile charge state increases from $Q = 26$ to $Q = 44$.

In order to partition E_{dep}, we use the functional dependence of stopping on Q and E for low energy ions from Refs. [14,15]. In the low kinetic energy regime ($E \approx 300$ keV), nuclear stopping is the most significant kinetic energy loss term for singly charged ions, and its magnitude is further increased when $Q \gg 1$. This increase arises from the enhancement of long range Coulomb

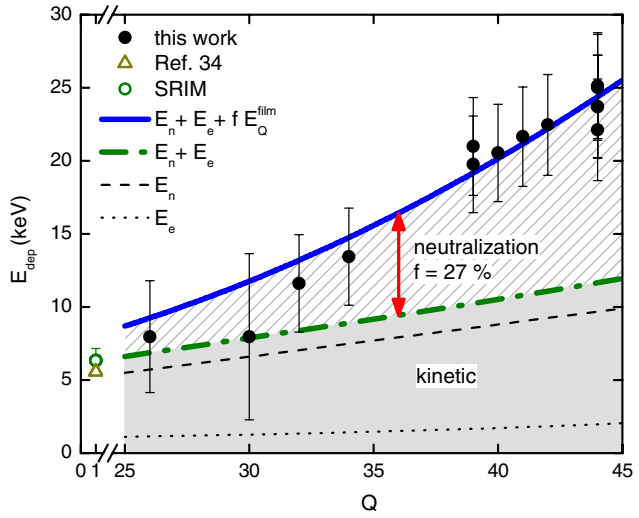

FIG. 3 (color online). Each point represents the energy required to form a crater, determined from a heated spike model. E_{dep} includes both kinetic $(E_n + E_e)$ and neutralization (E_Q^{film}) energy deposited within the thickness of the film. Error bars were determined by propagation of uncertainty in the data and model parameters. Total stopping from a previous experiment (△) [34] and SRIM (○) [7] at $E = 200$ keV $Q = 1$ are shown. Fitting the data with $E_{\mathrm{dep}} = E_n + E_e + fE_Q^{\mathrm{film}}$ gives the minimum fraction of neutralization energy $f = 0.27 \pm 0.02$ required for crater formation.

interactions which transfer small amounts of energy to large numbers of target atoms. Electronic stopping also increases with Q, but its value makes up only 7% of the total kinetic energy loss for the E and Q described here. Given the $Q = 1$ stopping powers from stopping range data [34] and the SRIM code [7] as well as the predicted functional dependence of electronic and nuclear stopping on Q and E at higher charge states [14], we find that the total (nuclear and electronic) kinetic energy loss per length $(dE_n/dz + dE_e/dz)$ increases from 0.5 to 0.8 keV Å^{-1} as the charge increases from $Q = 26$ to $Q = 44$. This equates to deposition of 7 to 12 keV kinetic energy into the thickness of the film $(E_n + E_e)$. Both E_n and E_e as well as their combined contributions to the energy deposition are plotted in Fig. 3.

As shown in Fig. 3, $E_{\mathrm{dep}}(Q)$ increases much more rapidly than the total kinetic energy loss $(E_n + E_e)$ as Q increases. Clearly, neutralization energy must be considered in order to account for the E_{dep} values. First, we estimate the amount of neutralization energy lost by the ion as it traverses the thickness of the film. Invoking an exponential charge state decay model [35,36], we calculate the charge state for a given ion that has traveled s_0 using the measured time constant from Ref. [22]. We then subtract the corresponding neutralization energies for this charge state and the initial charge state from one another to estimate the neutralization energy (E_Q^{film}) lost while the ion is within the film. E_Q^{film} represents the available neutralization energy that can contribute to heating the spike within the thickness s_0 and comprises more than 90% of E_Q as is displayed in the Fig. 2 inset. A fit to the data with the solid line $E_{\mathrm{dep}} = E_n + E_e + fE_Q^{\mathrm{film}}$ in Fig. 3 gives the fraction of available neutralization energy that contributes to formation of a crater to be $f = 0.27 \pm 0.02$. Uncertainty in f does not include a quantitative assessment of the error from the model in Ref. [14]. The fE_Q^{film} values are considered lower bounds on the total neutralization energy required to form the craters we observe in the Al_2O_3. In extracting f from the fit we assume that E_e and E_n are completely converted to heat in the collision spike. However for insulating materials, conversion of the electronic excitation to heat is not perfectly efficient [29], and its value will be smaller than the electronic stopping power integrated over the film thickness.

Schenkel and coworkers have reported that as much as 40% of the neutralization energy from Xe^{52+} projectiles is delivered into a Si detector target [19], where the remainder is emitted to the vacuum through Auger electrons and photons. We expect our measured fraction to be smaller than the result of Ref. [19], because craters only record the energy deposition that results in irreversible change of the material. Heated regions of the spike below the energy threshold for evaporation will quench and remain solid. The energy required for this subthreshold heating is transferred to the solid, but not represented in the measurement of a crater depth. Therefore, regarding the total energy deposited to the material, f quantifies the role that neutralization energy plays in the creation of irreversible defects.

In conclusion, we report the ion induced crater depths in ultrathin dielectric films as a function of projectile charge state. From the depth scaling of the craters with charge state, we determine the energy deposited into the thin film in HCI-surface impact increases from 8 to 25 keV as Q increases from 26 to 44. Accounting for both preequilibrium kinetic energy loss and neutralization energy, we measure that at least (27 ± 2)% of the available neutralization energy contributes to crater formation. This result represents a lower bound for the fraction of HCI neutralization energy required to form a permanent material defect.

R. E. L. and C. E. S. gratefully acknowledge support from NSF-CHE-0548111, Clemson University COMSET and NIST-60NANB9D9126.

*russell.lake@nist.gov

[1] H. J. Melosh and G. S. Collins, Nature (London) **434**, 157 (2005).
[2] A. S. El-Said *et al.*, Phys. Rev. Lett. **100**, 237601 (2008).
[3] R. Heller *et al.*, Phys. Rev. Lett. **101**, 096102 (2008).
[4] R. M. Papaléo *et al.*, Phys. Rev. Lett. **101**, 167601 (2008).
[5] E. Akcoltekin *et al.*, Nature Nanotech. **2**, 290 (2007).

[6] A. V. Krasheninnikov and K. Nordlund, J. Appl. Phys. **107**, 071301 (2010).
[7] J. Ziegler, J. Biersack, and U. Littmark, *The Stopping and Ranges of Ions in Matter* (Pergamon, New York, 1985).
[8] E. Chason *et al.*, J. Appl. Phys. **81**, 6513 (1997).
[9] C. Harrell, Z. Siwy, and C. Martin, Small **2**, 194 (2006).
[10] S. Facsko *et al.*, J. Phys. Condens. Matter **21**, 224012 (2009).
[11] F. Aumayr and H. P. Winter, Phil. Trans. R. Soc. A **362**, 77 (2004).
[12] J. M. Pomeroy *et al.*, Appl. Phys. Lett. **91**, 073506 (2007).
[13] Z. Insepov *et al.*, Nucl. Instrum. Methods Phys. Res., Sect. B **242**, 498 (2006).
[14] J. P. Biersack, Nucl. Instrum. Methods Phys. Res., Sect. B **80–81**, 12 (1993).
[15] T. Schenkel *et al.*, Phys. Rev. Lett. **79**, 2030 (1997).
[16] J. Burgdörfer, P. Lerner, and F. W. Meyer, Phys. Rev. A **44**, 5674 (1991).
[17] J. P. Briand *et al.*, Phys. Rev. Lett. **65**, 159 (1990).
[18] D. Kost *et al.*, Phys. Rev. Lett. **98**, 225503 (2007).
[19] T. Schenkel *et al.*, Phys. Rev. Lett. **83**, 4273 (1999).
[20] H. Kurz *et al.*, Phys. Rev. A **49**, 4693 (1994).
[21] Z. D. Pešić *et al.*, Phys. Rev. A **75**, 012903 (2007).
[22] M. Hattass *et al.*, Phys. Rev. Lett. **82**, 4795 (1999).
[23] A. E. T. Kuiper *et al.*, J. Appl. Phys. **89**, 1965 (2001).
[24] J. M. Pomeroy and H. Grube, Nucl. Instrum. Methods Phys. Res., Sect. B **267**, 642 (2009).
[25] J. M. Pomeroy and H. Grube, J. Appl. Phys. **105**, 094503 (2009).
[26] J. M. Pomeroy, R. E. Lake, and C. E. Sosolik, Nucl. Instrum. Methods Phys. Res., Sect. B **269**, 1238 (2011).
[27] E. L. Wolf, *Principles of Electron Tunneling Spectroscopy* (Oxford University Press, New York, 1985).
[28] H. Srikanth and A. K. Raychaudhuri, Phys. Rev. B **46**, 14 713 (1992); S. Ciraci and E. Tekman, Phys. Rev. B **40**, 11 969 (1989).
[29] M. Urbassek and P. Sigmund, Appl. Phys. A **35**, 19 (1984).
[30] P. Sigmund, Appl. Phys. Lett. **25**, 169 (1974).
[31] See Supplemental Material at http://link.aps.org/supplemental/10.1103/PhysRevLett.107.063202 for the derivation of Eq. (2).
[32] *CRC Handbook of Chemistry and Physics*, edited by W. M. Haynes (CRC Press/Taylor and Francis, Boca Raton, FL, 2011), 91st.
[33] G. P. Pells, J. Am. Ceram. Soc. **77**, 368 (1994).
[34] P. Jespersgaard and J. A. Davies, Can. J. Phys. **45**, 2983 (1967).
[35] R. Herrmann *et al.*, Phys. Rev. A **50**, 1435 (1994).
[36] K. Shima, N. Kuno, and M. Yamanouchi, Phys. Rev. A **40**, 3557 (1989).
[37] R. E. Lake, J. M. Pomeroy, and C. E. Sosolik, Nucl. Instrum. Methods Phys. Res., Sect. B **269**, 1199 (2011).